STATIC GROUND-STATE PROPERTIES OF THE 2D ELECTRON GAS

Paola Gori-Giorgi

Laboratoire de Chimie Théorique
CNRS and Université Pierre et Marie Curie
4 Place Jussieu, F-75252 Paris, France

Saverio Moroni, Giovanni B. Bachelet

INFM Center for Statistical Mechanics and Complexity
Dipartimento di Fisica, Università di Roma "La Sapienza"
Piazzale Aldo Moro 2, I-00185 Rome, Italy

1. INTRODUCTION

The two-dimensional electron gas (2DEG), realized in semiconductor heterostructures, has been a source of lasting inspiration for at least two generations of fundamental and applied researchers [1]. In recent years, for example, a new gold rush has been triggered by the experimental discovery of a metallic phase at low temperature [2], in contrast with the scaling theory of localization in two dimensions (2D) [3], and, independently, by the scientific and technological progress on quantum dots, which, at semiconductor interfaces, become nothing but tiny, quasi-two-dimensional quantum disks [4].

In this context, accurate predictions obtained from a simplified model, such as the ideal 2DEG (strictly 2D electrons interacting via a $1/r$ potential within a uniform, rigid neutralizing background), represent a valuable reference: the delicate interplay between electronic correlation and the effects of disorder can be better understood if, in the first place, accurate information on the *clean* system become available. Moreover, as in the three-dimensional case, the 2DEG ground-state properties are key ingredients in the construction of 2D exchange-correlation functionals for performing density functional theory (DFT) calculations e.g. on quantum dots [4,5,6].

With these two objectives in mind, i.e., to gain information on the ground-state phase diagram of the 2DEG, and, at the same time, to provide tools for perfoming DFT in two dimensions, we performed accurate diffusion Monte Carlo (DMC) calculations of the ground-state energy and of the pair-distribution functions of the 2DEG, and we parametrized our data with functional forms designed to satisfy all the known exact constraints. In this article we review our main results, and we deal with some aspects that went overlooked in our previous papers.

2. THE GROUND-STATE ENERGY AND THE PHASE DIAGRAM

The 2DEG model corresponds to N strictly 2D electrons confined in a square of surface S (periodically repeated in space) interacting via a $1/r$ potential within a uniform, rigid neutralizing background. When studying this model, one is usually interested in its macroscopic properties, i.e., the thermodynamic limit ($N, S \to \infty$ keeping $n = N/S$ constant) of its extensive physical quantities per particle. Two parameters are enough to define the 2DEG zero-temperature phase diagram, namely the density parameter $r_s = 1/\sqrt{\pi n} a_B^*$ (where n is the density and a_B^* is the effective Bohr radius) and the spin polarization $\zeta = (n_\uparrow - n_\downarrow)/n$, where $n_{\uparrow(\downarrow)}$ is the density of spin-up (down) electrons. Effective Hartree atomic units are used throughout this work.

Our calculations use standard fixed–node diffusion Monte Carlo (FN-DMC) [7], which projects the lowest-energy eigenstate Φ of the many-body Hamiltonian with the boundary condition that Φ vanishes at the nodes of a trial function Ψ. Details of the simulation are similar to those of Ref. [8]; further details can be found in Ref. [9]. For each of the densities corresponding to $r_s = 1, 2, 5, 10$ we have considered about 20 values of N and 10–12 polarizations ζ. For the densities $r_s = 20$ and 30 we have used the data of Ref. [8]. We have also computed the energy at $r_s = 40$ for $\zeta = 1$. To estimate the difference Δ between the energy $\epsilon_N(r_s, \zeta)$ of the finite system and its thermodynamic limit $\epsilon(r_s, \zeta)$ we adopted a new strategy. Rather than a separate size extrapolation for each density based on variational energies [10,11,12], we performed a global fit directly based on FN-DMC energies, which exploits two physically motivated ingredients: (i) the Fermi-liquid-like size correction [13]

$$\Delta(r_s, \zeta, N) = \epsilon_N(r_s, \zeta) - \epsilon(r_s, \zeta) = \delta(1+\lambda\zeta^2)[t_N(r_s, \zeta) - t_s(r_s, \zeta)] - (\eta + \gamma\zeta^2)/N \quad (1)$$

(t_N and t_s are the Fermi energies of N and ∞ particles, respectively, and $\delta, \lambda, \eta, \gamma$ are r_s-dependent parameters); (ii) an analytic expression for $\epsilon(r_s, \zeta)$ which involves 12 more free parameters (see below).

The only uncontrolled source of error, the fixed–node approximation, depends on the nodal structure of Ψ. We choose a Slater-Jastrow trial function with plane waves (PW) as single orbitals. However, within the fixed-node approximation, better results are obtained with backflow (BF) correlations in the wave function [12]. Since simulations with the BF wave function are considerably more demanding than with PW determinants, we calculated BF energies only for $\zeta = 0, N = 58$ and $\zeta = 1, N = 57$ for each density. For other values of N and ζ the effect of backflow is estimated as a quadratic interpolation in ζ and appended to PW energies, under the further assumption that the size dependence be the same for BF and PW [9].

The energy per electron in the thermodynamic limit $\epsilon(r_s, \zeta)$ is the sum of the non-interacting kinetic energy $t_s(r_s, \zeta) = (1 + \zeta^2)/2r_s^2$, the exchange energy $\epsilon_x(r_s, \zeta) =$

Table 1

Optimal fit parameters for the correlation energy, as parametrized in Eqs. (4)–(6). Values labelled with * are obtained from exact conditions

	$i=0$	$i=1$	$i=2$
A_i	-0.1925^*	0.117331^*	0.0234188^*
B_i	0.0863136^*	-3.394×10^{-2}	-0.037093^*
C_i	0.0572384	$-7.66765 \times 10^{-3*}$	0.0163618^*
D_i	$-A_0\,H_0$	$-A_1\,H_1$	$-A_2\,H_2$
E_i	1.0022	0.4133	1.424301
F_i	-0.02069	0^*	0^*
G_i	0.33997	6.68467×10^{-2}	0^*
H_i	1.747×10^{-2}	7.799×10^{-4}	1.163099
β	1.3386		

$-2\sqrt{2}[(1+\zeta)^{3/2}+(1-\zeta)^{3/2}]/3\pi r_s$, and the unknown correlation energy $\epsilon_c(r_s,\zeta)$. We built the function $\epsilon_c(r_s,\zeta)$ as an interpolation between the high-density expansion [14,15],

$$\epsilon_c(r_s \to 0,\zeta) = a_0(\zeta) + b_0(\zeta)\, r_s\, \ln(r_s) + O(r_s), \tag{2}$$

and the low-density (ζ-independent) limit [16],

$$\epsilon_c(r_s \to 0,\zeta) = -\frac{m}{r_s} + \frac{n}{r_s^{3/2}} + O\left(\frac{1}{r_s^2}\right), \tag{3}$$

that is

$$\epsilon_c(r_s,\zeta) = (e^{-\beta r_s} - 1)\epsilon_x^{(6)}(r_s,\zeta) + \alpha_0(r_s) + \alpha_1(r_s)\zeta^2 + \alpha_2(r_s)\zeta^4, \tag{4}$$

where

$$\epsilon_x^{(6)}(r_s,\zeta) = \epsilon_x(r_s,\zeta) - \left(1 + \frac{3}{8}\zeta^2 + \frac{3}{128}\zeta^4\right)\epsilon_x(r_s,0) \tag{5}$$

and the functions $\alpha_i(r_s)$ have the form

$$\alpha_i(r_s) = A_i + (B_i r_s + C_i r_s^2 + D_i r_s^3)\ln\left(1 + \frac{1}{E_i r_s + F_i r_s^{3/2} + G_i r_s^2 + H_i r_s^3}\right). \tag{6}$$

Notice that the value of the positive parameters m and n in Eq. (3) *do not* correspond to the Wigner crystal phase. They describe the low-density limit of the fluid phase, and are determined from a best fit to our data.

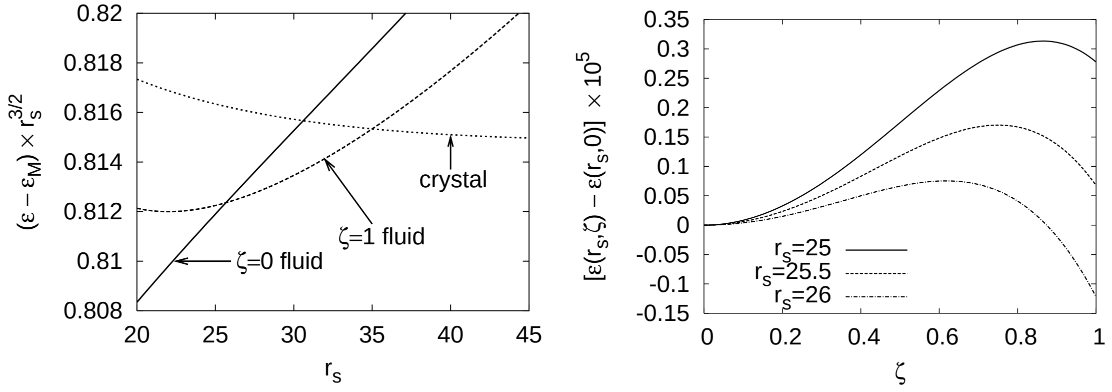

Figure 1. *Left panel:* the phase diagram of the 2D electron gas at zero temperature. The curve corresponding to the crystal phase is taken from Ref. [11], while the curves for the fluid phase are our parametrized data according to Eqs. (4)-(6). The Madelung energy ϵ_M is equal to $-1.1061/r_s$. *Right panel:* the transition to the fully polarized gas according to our simulation results and their corresponding parametrization.

The fitting parameters in Eqs.(4)-(6) (of which, only 12 are free, the other ones being fixed by exact conditions) are reported in Table 1. This analytic parametrization provides the local-spin density (LSD) functional for performing 2D DFT calculations. Saarikoski *et al.* [5] found that Eqs. (4)-(6) yield much better results in LSD calculations than previously proposed fomulas, and Kärkkäinnen *et al.* [17] have shown that a suitable analytic continuation of our functional form reasonably describes a multicomponent 2D electron gas.

In Fig. 1 we report the phase diagram of the 2DEG (left panel), and the analysis of the transition to the fully polarized gas (right panel). We see that this transition is weakly first order, being the energy differences on the y axis extremely tiny. However, we have to keep in mind that when the ζ-dependence of $\epsilon(r_s,\zeta)$ is extremely weak, the calculation of the small energy differences between the different phases could be biased by the fixed-node approximation, the assumption of quadratic contributions from BF correlation, and possible uncertainties from the size extrapolation, statistical noise, and the chosen functional form of ϵ_c. The very nature of the polarization transition, wealky first-order according to Fig. 1, is clearly based on the above approximations and assumptions.

3. PAIR-DISTRIBUTION FUNCTIONS

For an electronic system, the pair-distribution functions $g_{\sigma\sigma'}(\mathbf{r},\mathbf{r}')$, if $n_\sigma(\mathbf{r})$ is the density of electrons with spin $\sigma=\uparrow$ or $\downarrow$, are defined as

$$g_{\sigma\sigma'}(\mathbf{r},\mathbf{r}') = \frac{\langle\Phi|\psi^\dagger_\sigma(\mathbf{r})\psi^\dagger_{\sigma'}(\mathbf{r}')\psi_{\sigma'}(\mathbf{r}')\psi_\sigma(\mathbf{r})|\Phi\rangle}{n_\sigma(\mathbf{r})n_{\sigma'}(\mathbf{r}')}, \tag{7}$$

where $\psi^\dagger_\sigma$ and ψ_σ are the creation and annihilation field operators, respectively, and Φ is the ground-state wavefunction. The functions $g_{\sigma\sigma'}$ are thus related to the probability of finding two electrons of prescribed spin orientations at positions $\mathbf{r}$ and $\mathbf{r}'$. The normalization is such that the case of completely independent particles (without exchange and correlation) corresponds to the condition $g_{\sigma\sigma'} = 1$.

For a two-dimensional uniform electron gas, the functions $g_{\sigma\sigma'}$ only depend on $r = |\mathbf{r} - \mathbf{r}'|$, and parametrically on the density parameter r_s and on the spin-polarization parameter ζ. The total (spin-summed) pair-distribution function is defined as

$$g = \left(\frac{1+\zeta}{2}\right)^2 g_{\uparrow\uparrow} + \left(\frac{1-\zeta}{2}\right)^2 g_{\downarrow\downarrow} + \frac{1-\zeta^2}{2} g_{\uparrow\downarrow}. \tag{8}$$

An accurate knowledge of these functions for the 2DEG and their avalaibility in analytic form (parametrization) may serve a variety of purposes: the exchange-correlation hole and its dependence on the electron density and spin polarization may be relevant to the physics of the metal-insulator transition in 2D [18] and to self-energy theories of the 2DEG [19], but is also needed for the estimate of the effects of the finite thickness on the spin susceptibility [20] and for the construction of generalized-gradient approximations (GGA) or weighted-density approximations (WDA) of density functionals, in analogy to the 3D case [21,22]. The availability of density functionals better than local-spin-density (LSD) approximations for the 2DEG would, in turn, allow an almost exact description of quantum dots, since the spatial variation of their carrier density is rather weak [4,5,6].

We performed Reptation Monte Carlo (RMC) simulations [23], and we obtained the spin-resolved pair-distribution functions by averaging $V dN_{\sigma\sigma'}(r')/[N_\sigma(N_{\sigma'} - \delta_{\sigma\sigma'})2\pi r\Delta]$ in the middle slice of the path during the simulation, where V is the volume of the simulation cell and $dN_{\sigma\sigma'}(r')$ is the number of electron pairs with distance r' between $r - \Delta/2$ and $r + \Delta/2$. In our calculations the total number of particles is 42, 50, 50 and 45 for polarization 0, 0.48, 0.80 and 1, respectively. By repeating simulations for different system sizes in the unpolarized case, finite size effects on the pair-distribution function have been estimated to be of order 0.01. All the other systematic errors (except the uncontrolled fixed-node approximation) are kept within this level. Following the same strategy adopted for the energy calculation, we considered two different nodal structures: plane waves and backflow. The difference bewteen the two is found to be within our targeted accuracy of 0.01 [24]. A sample of our data is shown in Fig. 2.

The data for the spin-summed g of Eq. (8) have been parametrized with a three-variable function $g(r, r_s, \zeta)$ that embodies exact properties for small and large inter-electronic distances, as well as exact sum rules [24]. Via the virial theorem,

$$\frac{k_{\mathrm{F}}}{2}\int_0^\infty dx\, g^c(x, r_s, \zeta) \equiv v_c(r_s, \zeta) = \frac{1}{r_s}\frac{\partial}{\partial r_s}\left[r_s^2 \epsilon_c(r_s, \zeta)\right], \tag{9}$$

our parametrized g is also constrained to be consistent with the correlation energy computed in the previous section. In Eq. (9) $x = k_{\mathrm{F}} r$ is a scaled variable, and k_{F} is the Fermi wavevector of the unpolarized gas, $k_{\mathrm{F}} = \sqrt{2}/r_s$. The function g^c is the correlation part of $g = g^x + g^c$, where g^x is the well-known exhange-only pair-distribution function [24].

For the spin-resolved $g_{\sigma\sigma'}$ fewer exact properties are known, and we succeeded only to parametrize our data for the unpolarized gas ($\zeta = 0$) and for $r_s \le 10$ [24].

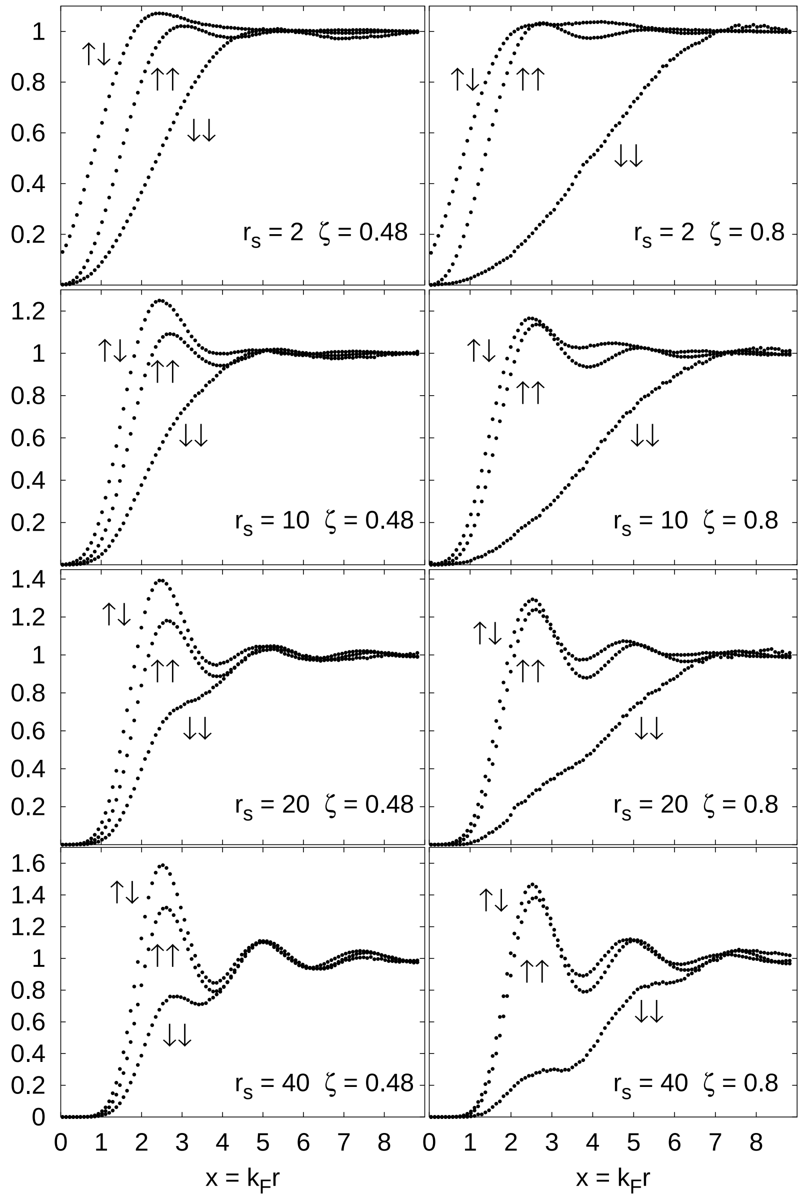

Figure 2. A sample of the Reptation Monte Carlo pair-distribution functions $g_{\sigma\sigma'}$ of the 2D electron gas for different densities and spin polarizations. Here $k_{\rm F}$ is the Fermi wavevector of the unpolarized gas, $k_{\rm F} = \sqrt{2}/r_s$.

4. SPIN-RESOLVED POTENTIAL ENERGY

The correlation part of the potential energy, $v_c(r_s, \zeta)$ of Eq. (9), can be divided into $\uparrow\uparrow$, $\downarrow\downarrow$, and $\uparrow\downarrow$ contributions, such that $v_c = v_c^{\uparrow\uparrow} + v_c^{\downarrow\downarrow} + v_c^{\uparrow\downarrow}$. These spin-resolved components of v_c are important ingredients for the study and construction of dynamical exchange-correlation potentials in the spin channel [25,26]. They can

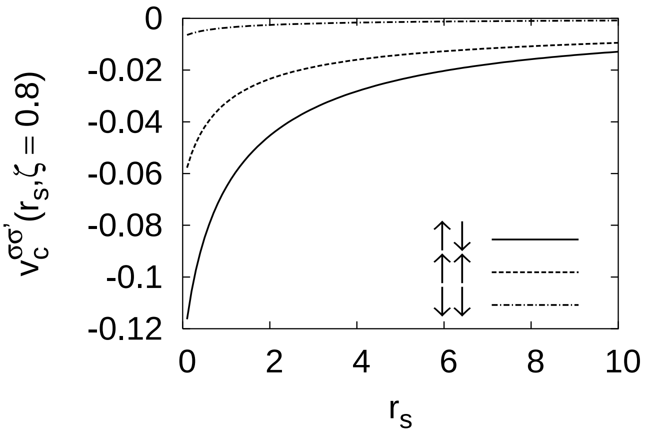

Figure 3. The spin-resolved potential energy of correlation $v_c^{\sigma\sigma'}$ for $\zeta = 0.8$, as a function of the density parameter r_s.

be written as the expectation value of the Coulomb potential $1/r$ on the spin-resolved $g^c_{\sigma\sigma'}$,

$$v_c^{\sigma\sigma'}(r_s,\zeta) = \frac{(2-\delta_{\sigma\sigma'})}{\sqrt{2}\,r_s}\frac{n_\sigma n_{\sigma'}}{n^2}\int_0^\infty g^c_{\sigma\sigma'}(x,r_s,\zeta)\,dx. \tag{10}$$

We have evaluated the r.h.s. of Eq. (10) by numerical integration of our QMC data for $g^c_{\sigma\sigma'}(x,r_s,\zeta)$, at $\zeta = 0, 0.48, 0.8$, and $r_s = 1, 2, 5, 10, 20, 40$. The results have been parametrized as [27]

$$v_c^{\sigma\sigma'}(r_s,\zeta) = F_{\sigma\sigma'}(r_s,\zeta)\,v_c(r_s,\zeta). \tag{11}$$

The fractions $F_{\sigma\sigma}(r_s,\zeta)$ for parallel spins are well represented by

$$F_{\uparrow\uparrow}(r_s,\zeta) = F^{\rm HD}_{\uparrow\uparrow}(\zeta) + \left[w_1(\zeta)\,r_s + w_2(\zeta)\,r_s^2\right]\ln\left(1+\frac{w_3(\zeta)}{r_s^2}\right), \tag{12}$$

where the high-density $F^{\rm HD}_{\uparrow\uparrow}$ is given by Seidl [14]

$$F^{\rm HD}_{\uparrow\uparrow}(\zeta) = \frac{-19.54\,(1+\zeta)}{153.38\mathcal{F}(\zeta)-192.46}, \tag{13}$$

and

$$\mathcal{F}(\zeta) = \frac{(1+\zeta)\log(1+\zeta)+(1-\zeta)\log(1-\zeta)}{2\log(2)} + 0.0636\,\zeta^2 - 0.1024\,\zeta^4 + 0.0389\,\zeta^6. \tag{14}$$

The functions $w_i(\zeta)$ have been obtained by fitting our data for $v_c^{\uparrow\uparrow}(r_s,\zeta)$ for $\zeta = -0.8, -0.48, 0., 0.48, 0.8$ (the negative ζ values corresponding to the $\downarrow\downarrow$ data), $w_1(\zeta) = (1-\zeta)\,(-0.006 - 0.03\,\zeta)$, $w_2(\zeta) = (1-\zeta)\,(-0.01 + 0.03\,\zeta)$, and $w_3(\zeta) = 3.6\,(1+\zeta)^4$. Equation (12) completely determines the spin resolution of $v_c(r_s,\zeta)$, since $F_{\downarrow\downarrow}(r_s,\zeta) = F_{\uparrow\uparrow}(r_s,-\zeta)$ and $F_{\uparrow\downarrow} = 1 - F_{\uparrow\uparrow} - F_{\downarrow\downarrow}$.

In Fig. 3 we show the spin-resolved potential energy of correlation $v_c^{\sigma\sigma'}$ for $\zeta = 0.8$, as a function of the density parameter r_s. We see that even for values of ζ

close to 1 (i.e., close to the fully polarized case) v_c is dominated by the antiparallel-spin contribution. This effect is stronger than in the 3D case [27] because in two dimensions the short-range contribution to the energy is larger.

5. CONCLUSIONS AND PERSPECTIVES

We have reviewed and further analyzed our results for the static ground-state properties of the 2D electron gas. Future work will be devoted to the calculation of the spin-resolved ($\uparrow$ and $\downarrow$) kinetic energies following a technique suggested by Dobson, Le and Vignale [28], the construction of a generalized gradient approximation density functional for 2D, and the study of response functions.

ACKNOWLEDGMENTS

The research described herein was supported by the Italian Ministry of Education, University and Research (MIUR) through COFIN 2003-2004 and by the allocation of computer resources from INFM Iniziativa Calcolo Parallelo. P.G.-G. gratefully acknowledges the U.S. National Science Foundation, through Grant No. DUE-0127488 to the Shodor Education Foundation for supporting her partecipation to the Workshop "Condensed Matter Theories XXVIII".

REFERENCES

[1] see e.g. T. Ando, A. B. Fowler, and F. Stern, *Rev. Mod. Phys.* **54**, 437 (1982); E. Abrahams, S. V. Kravchenko M. P. Sarachik, *Rev. Mod. Phys.* **73**, 251.

[2] S. V. Kravchenko and M. P. Sarachik, *Rep. Prog. Phys.* **67**, 1 (2004).

[3] E. Abrahams, P. W. Anderson, D. C. Licciardello, and T. V. Ramakrishnan, *Phys. Rev. Lett.* **42**, 673 (1979)

[4] S.M. Reimann and M. Manninen, *Rev. Mod. Phys.* **74**, 1283 (2002).

[5] H. Saarikoski, E. Räsänen, S. Siljamäki, A. Harju, M. J. Puska, and R. M. Nieminen, *Phys. Rev. B* **67**, 205327 (2003).

[6] H. Jiang, H.U. Baranger, and W. Yang, *Phys. Rev. B* **68**, 165337 (2003).

[7] W. M. C. Foulkes, L. Mitas, R. J. Needs and G. Rajagopal, *Rev. Mod. Phys.* **73** 33 (2001).

[8] D. Varsano, S. Moroni, and G. Senatore, *Europhys. Lett.* **53**, 348 (2001).

[9] C. Attaccalite, S. Moroni, P. Gori-Giorgi, and G.B. Bachelet, *Phys. Rev. Lett.* **88**, 256601 (2002); **91**, 109902(E) (2003).

[10] B. Tanatar and D. M. Ceperley, *Phys. Rev. B* **39**, 5005 (1989).

[11] F. Rapisarda and G. Senatore, *Aust. J. Phys.* **49**, 161 (1996).

[12] Y. Kwon, D. M. Ceperley, and R. M. Martin, *Phys. Rev. B* **58**, 6800 (1998).

[13] D.M. Ceperley, *Phys. Rev. B* **18**, 3126 (1978).

[14] M. Seidl, *Phys. Rev. B* **70**, 073101 (2004).

[15] A. K. Rajagopal, J. C. Kimball, *Phys. Rev. B* **15**, 2819 (1977).

[16] L. Bonsall and A.A. Maradudin, *Phys. Rev. B* **15**, 1959 (1977).

[17] K. Kärkkäinen, M. Koskinen, S. M. Reimann, and M. Manninen, *Phys. Rev. B* **68**, 205322 (2003).

[18] D.J.W. Geldart and D. Neilson, *Phys. Rev. B* **67**, 045310 (2003).

[19] M. Vogt, R. Zimmermann and R. J. Needs, *Phys. Rev. B* **69**, 045113 (2004).

[20] S. De Palo, M. Botti, G. Senatore, and S. Moroni, cond-mat/0410145.

[21] J.P. Perdew, in *Electronic Structure of Solids '91*, edited by P. Ziesche and H. Eschrig (Akademie Verlag, Berlin 1991); J.P. Perdew, K. Burke, and Y. Wang, *Phys. Rev. B* **54**, 16533 (1996).

[22] Z. Wu, R.E. Cohen, and D.J. Singh, *Phys. Rev. B* **70**, 104112 (2004).

[23] S. Baroni and S. Moroni, *Phys. Rev. Lett.* **82**, 4745 (1999).

[24] P. Gori-Giorgi, S. Moroni, and G.B. Bachelet, *Phys. Rev. B* **70**, 115102 (2004).

[25] Z. Qian and G. Vignale, *Phys. Rev. B* **68**, 195113 (2003).

[26] Z. Qian, cond-mat/0404325.

[27] P. Gori-Giorgi and J.P. Perdew, *Phys. Rev. B* **69**, 041103(R) (2004).

[28] J.F. Dobson, H.M. Le, and G. Vignale, *Phys. Rev. B* **70**, 205126 (2004).